# Characterization and modeling of the moisture diffusion behaviour of natural fibres

Amandine Célino, Sylvain Fréour, Frédéric Jacquemin, Pascal Casari

# Characterization and Modeling of the Moisture Diffusion Behavior of Natural Fibers

**Amandine Célino, Sylvain Fréour, Frédéric Jacquemin, Pascal Casari**

Institut de Recherche en Génie Civil et Mécanique (UMR CNRS 6183), LUNAM Université - Université de Nantes - Centrale Nantes, CRTT, 37 Boulevard de l'Université, BP 406, 44602 Saint-Nazaire cedex, France

Correspondence to: A. Célino (E-mail: amandine.celino@univ-nantes.fr)

**ABSTRACT:** Natural fibers have good properties to be used as reinforcement in composite materials. The main issue is their hydrophilic behavior. So we propose here to investigate the diffusion phenomenon in such fibres. First, a brief characterization of four vegetal fibers has been achieved. We show that all fibers have a similar composition and structure despite their different origin. Then, their moisture diffusive behavior was investigated. The samples were submitted to hygro-thermal aging either in total water immersion at room temperature or in an environmental chamber at 80% relative humidity and 23°C. Various predictive models were used to simulate experimental curves. Results show that all fibers exhibit a similar diffusive behavior in a same environment. In immersion, specimens show anomalous absorption kinetics and Langmuir theory actually describes very well the diffusion kinetics in such conditions, whereas the same fibers follow a Fickian diffusion when they are exposed to vapor during relative humidity aging.

**KEYWORDS:** cellulose and other wood products; fibers; aging; properties and characterization; theory and modeling

## INTRODUCTION

Since several years, with the growth of the environmental concern, bio-based materials have been more extensively studied for specific applications. In the field of composite materials, natural fibers are actually considered as a possible alternative to glass fibers for reinforcing polymeric matrix in automotive engineering, particularly.[1–3] They are light, abundant, and renewable. Moreover, they exhibit higher specific mechanical properties than glass fibers because of their low density.[4] The main issue related to the use of plant fibers is their hydrophilic behavior because of free hydroxyl groups. Understanding the interactions between natural fibers and water is of great importance, because of the pronounced influence of moisture on their mechanical properties as well as on dimensional changes.[5,6] Therefore, the adhesion with hydrophobic matrix is not strong enough and the aging of composite materials reinforced by plant fibers can lead to a premature degradation and the loss of their mechanical properties.[7,8] Many practical investigations have been achieved to modify the structure of natural fibers in order to reduce their hydrophilic characteristic.[9–12] However, few people have explored the diffusion phenomenon inside these fibers to understand the mechanism of moisture absorption.[13,14] Various physical models describing diffusion phenomenon inside polymers are available in literature. Among them, Fick's law is the most common model used.[15,16] However, some polymers present anomalous Fickian diffusion.[17,18] In these cases, others models can be used as Langmuir theory[19] or a dual-stage Fick's law.[20] In the purpose of bio-based fibres, more recently, Kohler et al. used a mathematical equation to describe kinetics of water vapor sorption inside cellulosic fibers.[21] The numerical fitting proposed in the article does not enable the identification of diffusion parameters nor the prediction of the moisture content spatial distribution along thickness as in classical models. Yet, this is of great importance to study the mechanical states inside materials in the transient state. As an example, Ref. 22 constitutes an interesting theoretical work where the authors determined the spatial distribution of moisture content inside cylindrical material and the resulting mechanical stresses by using both a Fickian and a hygroelastic model.

In the present work, we intend to use these classical diffusion models on four natural fibers diffusion kinetics. In a first time, a characterization of our fibers has been achieved. Fourier transform infrared spectroscopy (FTIR spectroscopy) analysis allowed investigating the composition, X-ray diffraction enabled to quantify the crystallinity, while scanning electron microscopy (SEM) was used to observe the surface morphology. Eventually, fiber densities were determined owing to pycnometry. In a second time, kinetics diffusion of the fibers was independently

Table I. Mechanical Properties of Different Fibers[23,24,28]

| | Density ($g/cm^3$) | Specific stress ($MPa.cm^3/g$) | Specific young modulus ($GPa.cm^3/g$) |
|---|---|---|---|
| Flax | 1.4-1.55 | 238-1000 | 34-76 |
| Hemp | 1.4-1.5 | 214-1264 | 24-50 |
| Jute | 1.3-1.46 | 286-650 | 7-22 |
| E-Glass | 2.55 | 941 | 29 |

studied in vapor humidity and liquid water. Experimentally, the samples were submitted to hygro-thermal aging, either through liquid water immersion at room temperature or in an environmental chamber at 80% relative humidity and 23°C. Periodic gravimetric measurements were achieved on the specimens in order to study the weight gain as a function of the time. Numerical modeling was intended to identify the diffusive parameters of each fiber and provide an enhanced understanding of the mechanism of moisture absorption inside such bio-based constituents.

## MATERIALS AND METHODS

### Materials

Fibers studied are hemp, flax, jute, and sisal. Among plant fibers, these one's present the best mechanical properties regarding glass fibers replacement for the purpose of reinforcing polymeric matrix (Table I).[23,24,28] Flax, hemp, and jute are extracted from the stem of the plant whereas sisal is extracted from the leaf. As shown in Figure 1, plant fibers have a multiscale structure. Thus, the diffusion of water is influenced by the fiber structure at different scales. In the unit fiber scale, the fiber exhibits a complex multi-cell wall structure [Figure 1(c)]. This structure can in first approximation be assumed to behave similarly to its higher layer S2, which usually constitutes more than 80% of the total diameter [Figure 1(d)].[25] Actually, this layer is assumed to be a composite material with an amorphous phase (matrix) reinforced by a rigid crystalline phase (cellulose microfibrils).[26] At this scale, diffusion of water would take place in the amorphous region. Besides, these regions are mainly composed by hydrophilic polymers (hemicelluloses and lignin). In the bundle scale [Figure 1(b)], diffusion is privileged trough the interface between fibers "the middle lamella." According to Morvan et al.[27], the middle lamella is principally composed of pectin where the carboxyl functions make easier the absorption of water by hydrogen bonding. The last structural factor influencing diffusion is the general porous structure of natural fibers. Water could be trapped inside pores.

In the following study, bundles of hemp, flax, jute, and sisal fibers have been characterized.

### Characterization

**Fourier Transform Infrared Spectroscopy.** To compare their composition, we carried out FTIR on the four fibers in ambient conditions. Bundles were submitted to FTIR spectrometer using a Bruker Tensor 27 stage operating in attenuated total reflectance (ATR) mode with a diamond crystal. Scanning was conducted in the frequency range 4000–400 $cm^{-1}$ with a 32 repetitions scan average for each sample and a resolution of 2 $cm^{-1}$. Spectra were baseline corrected.

As the molecule in the cellulose chain will vibrate differently in well-ordered crystalline phases compared to less-ordered phases, it is possible to assign absorption band to crystalline and amorphous region.[29]. Then a crystallinity index could be evaluated. In this study, lateral order index (LOI)[30] and total crystallinity index (TCI)[31] established in the 60s have been calculated. For LOI, ratio between the absorption band at 1429 $cm^{-1}$ characteristic of cellulose crystalline phase and the absorption band at 897 $cm^{-1}$ from the amorphous phase has been used. In the same way, ratio between the absorption bands at 1375 and 2900 $cm^{-1}$ allowed the determination of TCI. These results have been compared to crystallinity indices obtained by Segal's method using X-ray analysis (see section "X-ray diffraction").

**X-Ray Diffraction.** Native cellulose, which consists of an alternation of amorphous and crystalline regions, is the main constituent of natural fibers. As it is the only element to crystallize in natural fibers, it is possible to evaluate the crystallinity rate in such fiber by doing X-Ray diffraction analysis.

X-ray diffractograms were recorded on a Seifert 3003 PTS diffractometer using Cu K$\alpha$ radiation ($\lambda = 1.504018$ Å). The diffractometer was used in the symmetrical transmission mode and the intensity was measured as a function of the scattering angle $2\theta$ by $\theta - 2\theta$ scan. Analysis was realized in $2\theta$ from 10° until 60° with a step of 0.15° and a delay time of 5 s. Spectral analysis was done in the longitudinal and transversal side. For illustration, flax bundle sample used is depicted in Figure 2. By using empirical method based on Segal et al.'s works,[32] we calculated the crystallinity degree of the four fibers. Among the different methods developed to determine crystallinity index by X-ray analysis and compared in Thygesen et al.'s works,[33] Segal's method is the simplest, fastest, and more frequently used method. Results give

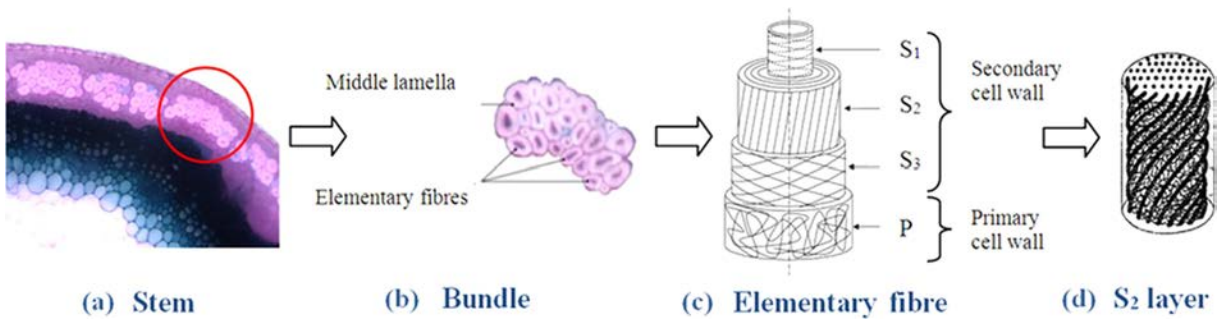


Figure 1. Multiscale structure of the flax fiber.[26,27,28] [Color figure can be viewed in the online issue, which is available at wileyonlinelibrary.com.]

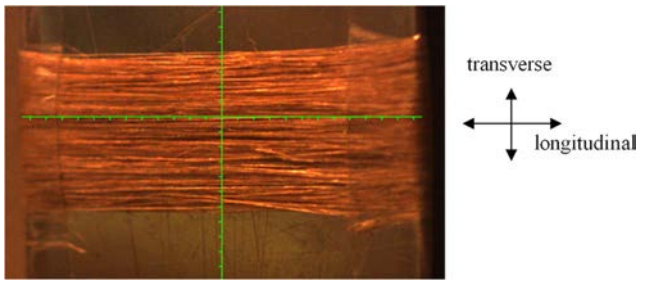


**Figure 2.** Flax sample used for X-Ray analysis. [Color figure can be viewed in the online issue, which is available at wileyonlinelibrary.com.]

qualitative or semi-quantitative information. In practice, sample crystallinity, Xcr, is determined by eq. (1) using the height of the (002) peak ($I_{002}$, $2\theta = 22.6°$) and the minimum between the (002) and 110 peaks ($I_{AM}$, $2\theta = 18°$) (Figure 3). $I_{002}$ represents the contribution from both crystalline and amorphous materials while $I_{AM}$ represents amorphous material only.

**Scanning Electron Microscopy.** The fibers morphologies were investigated by SEM using an environmental microscope EVO40 EP from CARL ZEISS Company.

**Pycnometry.** Densities of the four dried fibers were determined using the classical liquid pycnometry method.[34]

**Specimen Aging.** To study the diffusive behavior of the four fibers, bundles were submitted to hygro-thermal aging either in total water immersion at room temperature or in an environmental chamber at 80% relative humidity and 23°C. Absorption or desorption kinetics has been plotted by doing periodic gravimetric measurements.

In the case of immersion experiments, as it is technically difficult to periodically weigh fibers in liquid water, desorption kinetics has been studied. Thereby, each specimen (Figure 4) was first immersed in distilled water at room temperature during 11 days until saturation is reached. Then, they were dried in a desiccators

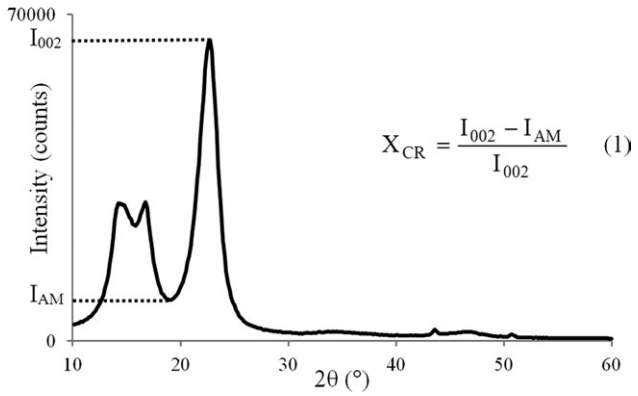


**Figure 3.** Segal method.

containing silica gel (RH = 7.5%) and kept in room temperature. During drying, the samples were periodically weighed in order to study the weight loss as a function of the time. Data were read to 0.01 mg in a precision balance. The moisture content ($M_w$) is calculated at several times and is expressed in terms of mass percentage as follows in order to obtain time-dependent desorption curves for each fiber:

$$M_w(\%) = \frac{M(t) - M_0}{M_0} \times 100 \quad (2)$$

where $M_0$ is the initial weight of the bulk specimens before immersion (ambient conditions) and $M(t)$ is the weight of the specimen at time $t$.

In the case of relative humidity aging, specimens were kept in a climatic chamber with RH = 80% and $T = 23°C$. Sorption kinetics has been followed using gravimetry.

## RESULTS AND DISCUSSION

### Characterization

**FTIR Spectroscopy.** The chemical composition of hemp, jute, flax, and sisal fibers was analyzed using FTIR-ATR. The

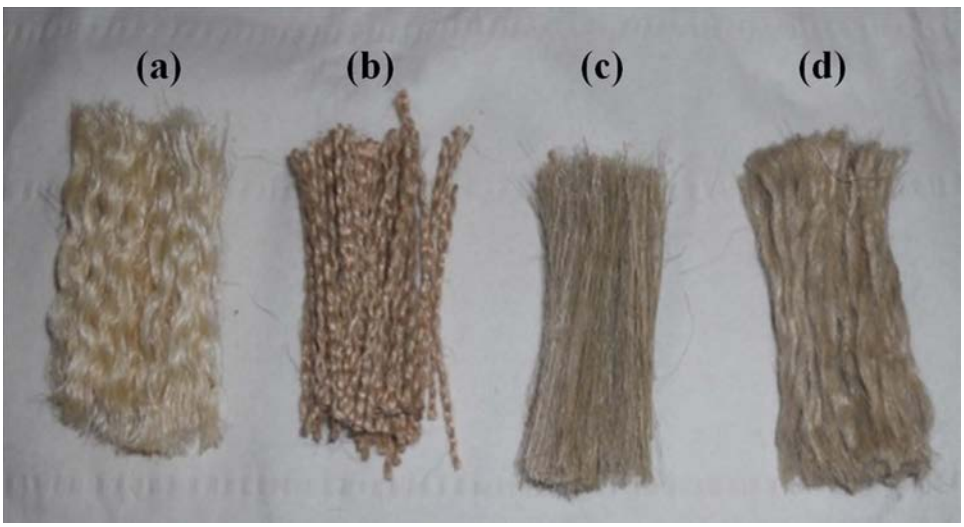


**Figure 4.** Specimens aged in hygrothermal environments (a) sisal, (b) jute, (c) flax, (d) hemp. [Color figure can be viewed in the online issue, which is available at wileyonlinelibrary.com.]

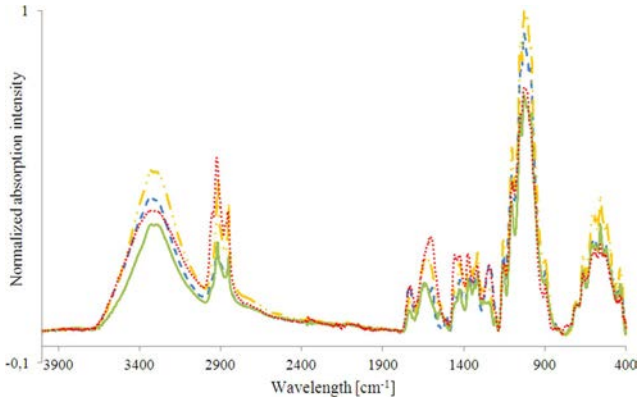


**Figure 5.** FTIR spectra of ··· sisal, --- jute, —·· flax, and — hemp fibers. [Color figure can be viewed in the online issue, which is available at wileyonlinelibrary.com.]

interesting peaks have been identified on Figure 5. They are summarized in Table II through literature.[35–39] The four fibers have a similar chemical footprint. Absorption band characteristics of lignin, cellulose, and hemicelluloses have been identified (Table II).

The broad absorption band between 3600 and 3000 $cm^{-1}$ is the characteristic of the O—H stretching vibration and hydrogen bond of the hydroxyl groups assigned, by deconvolution, to intramolecular or intermolecular hydrogen bonding and free OH hydroxyl.[38] This unstructured absorption band is indirectly linked by water content. Indeed, in a recent work, Olsson and Salmèn,[40] studied the effect of water on the FTIR spectra of paper. They showed two peaks in the OH-valency region directly affected by water (at 3600 and 3200 $cm^{-1}$). They supposed that the peak observed at 3200 $cm^{-1}$ could be associated with strongly bound water (water bound directly by hydrogen bonds to the OH groups of cellulose and the hemicelluloses) and the peak at 3600 $cm^{-1}$ is associated with more loosely bound water, that is, water indirectly bonded to the OH groups via another water molecule.

The absorption band at 1635 $cm^{-1}$ is assigned by several authors to be characteristic of adsorbed water.[35,37] This peak testifies the presence of water in the samples. Indeed, in ambient conditions natural fibers contain residual water.

Actually, the principal information, given by the experiment, is first the similarity between each fibers and, second, the spectral footprint of the fibers testifying the presence of hydroxyl and carboxyl functions, which lead to moisture absorption in such fibers.[41,42]

The LOI and the TCI were calculated using the concerned absorption peaks from the infrared spectra. Results are presented in Table III. The two ratios do not give the same result for a same sample. LOI results show, hemp, flax, and jute have a significantly higher crystallinity index than sisal, whereas TCI results show jute sample has a higher crystallinity index than the three other fibers. This last result cannot correlate with cellulose content in such fibers. Indeed, according to literature, cellulose content is higher in flax and hemp fibers than in the two others. Thus, crystallinity should be higher for these two fibers than jute and sisal as it is the case for results obtained with LOI ratio. It should be noted that this method could introduce some errors because the spectrum analyzed contains contribution from both crystalline and amorphous phases of the samples.

**Table II.** Assignment of the Main Absorption Bands in FTIR Spectra of Sisal, Jute, Flax, and Hemp Fibers[34–38]

| Wavelenght ($cm^{-1}$) | Assignment |
|---|---|
| 3600-3100 | Intra and inter molecular Hydrogen bonding of OH stretching in cellulose, hemicelluloses |
| 2955 | CH stretching of cellulose and hemicellulose |
| 2935 | CH stretching of cellulose and hemicellulose |
| 2862 | $CH_2$ stretching of cellulose and hemicellulose |
| 1735 | C=O stretching acetyl or carboxylic acid |
| 1635 | Adsorbed water |
| 1595 | Aromatic ring in lignin (exclusively in jute spectrum) |
| 1502 | Aromatic ring in lignin (exclusively in jute spectrum) |
| 1460 | OH in plan bending |
| 1425 | Carboxylic acid and COO— vibration |
| 1375 | CH bending of cellulose and hemicellulose |
| 1335 | OH in plane deformation |
| 1315 | $CH_2$ wagging of cellulose and hemicellulose |
| 1275 | Lignin (jute and sisal spectrum) |
| 1245 | C—O of acetyl (hemicelluloses or pectin) |
| 1200 | OH in plane bending |
| 1150 | Anti-symmetrical deformation of the C—O—C band |
| 1125-895 | C—O stretching and ring vibrational modes |
| 900 | Characteristic of β-links in cellulose |
| 700-650 | OH out of plane bending |

**X-ray Scattering.** In the X-ray diffractograms, presented in Figure 6, three peaks were observed for all samples. They are characteristic of the native cellulose crystalline structure $I_\beta$.[43] The peak at $2\theta = 14.9°$ corresponds to the (110) crystallographic plane, the other one at $2\theta = 16.5°$ corresponds to $(1\bar{1}1)$ plane and the peak at $2\theta = 22.6°$ corresponds to the (002) reflection.

The crystallinity indices were obtained from X-ray diffractograms according to the method based on the intensity measured at two

**Table III.** Crystallinity Indices of the Fibers Calculated from IR Spectra

| | LOI | TCI |
|---|---|---|
| Sisal | 0.725 ± 0.031 | 0.335 ± 0.021 |
| Jute | 1.261 ± 0.017 | 0.632 ± 0.023 |
| Flax | 1.459 ± 0.060 | 0.384 ± 0.016 |
| Hemp | 1.301 ± 0.008 | 0.459 ± 0.033 |

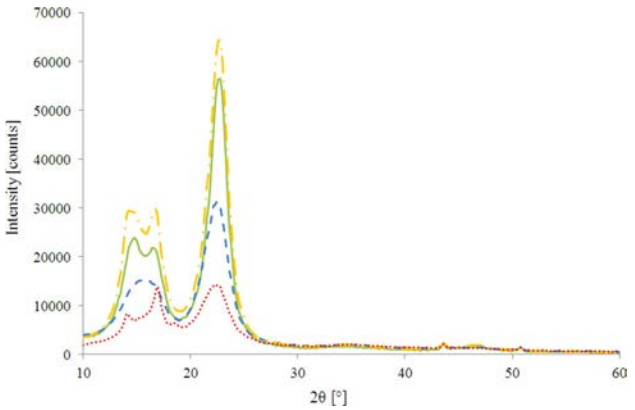


**Figure 6.** X-ray diffractogramms of the four fibers (··· sisal, --- jute, —·· flax, — hemp). [Color figure can be viewed in the online issue, which is available at wileyonlinelibrary.com.]

points in the diffractogram, proposed by Segal et al.[32] They were calculated in both the longitudinal ($\Psi = 0°$) and transverse ($\Psi = 90°$) directions. Results are displayed in Table IV.

The X-ray results show two groups of fibers. Hemp and flax fibers have a main crystallinity index of 88% higher than those of the two other fibers. They are about 10% superior to jute crystallinity index in both directions and about 30% and 15% superior to sisal crystallinity index in longitudinal and transversal direction, respectively. Results obtained for a given fiber are almost the same in longitudinal or transversal direction except

**Table IV.** Crystallinity Indices of the Fibers in Longitudinal $\Psi = 0°$ and Transversal $\Psi = 90°$ Direction

| | $\Psi = 0°$ (%) | $\Psi = 90°$ (%) |
|---|---|---|
| Sisal | 58 | 73 |
| Jute | 78.4 | 79.9 |
| Flax | 87 | 88 |
| Hemp | 88.1 | 88.2 |

for sisal. Indeed, in the longitudinal direction, crystallinity index calculated for sisal fibers has to be considered with critical mind. Compared to other fibers, sisal was difficult to handle and a defect in the sample flatness could lead to an incorrect measurement.

Results obtained are overestimated because of some weakness in the method as reported by some authors.[33,44] Actually, cellulose content in such fibers is reported to be 78% in flax, for example.[45] As a consequence, the method gave us only semi-quantitative information to compare the four fibers together. These results show a good correlation with LOI ratio calculated from the IR spectra. According to Nakamura et al.,[46] diffusion coefficient inside cellulosic materials have a strong relationship with the amorphous fraction of cellulose, as the water molecule can diffuse only through the amorphous part of cellulose samples. Thereby, moisture absorption should be more important in sisal or jute than in the two others fibers.

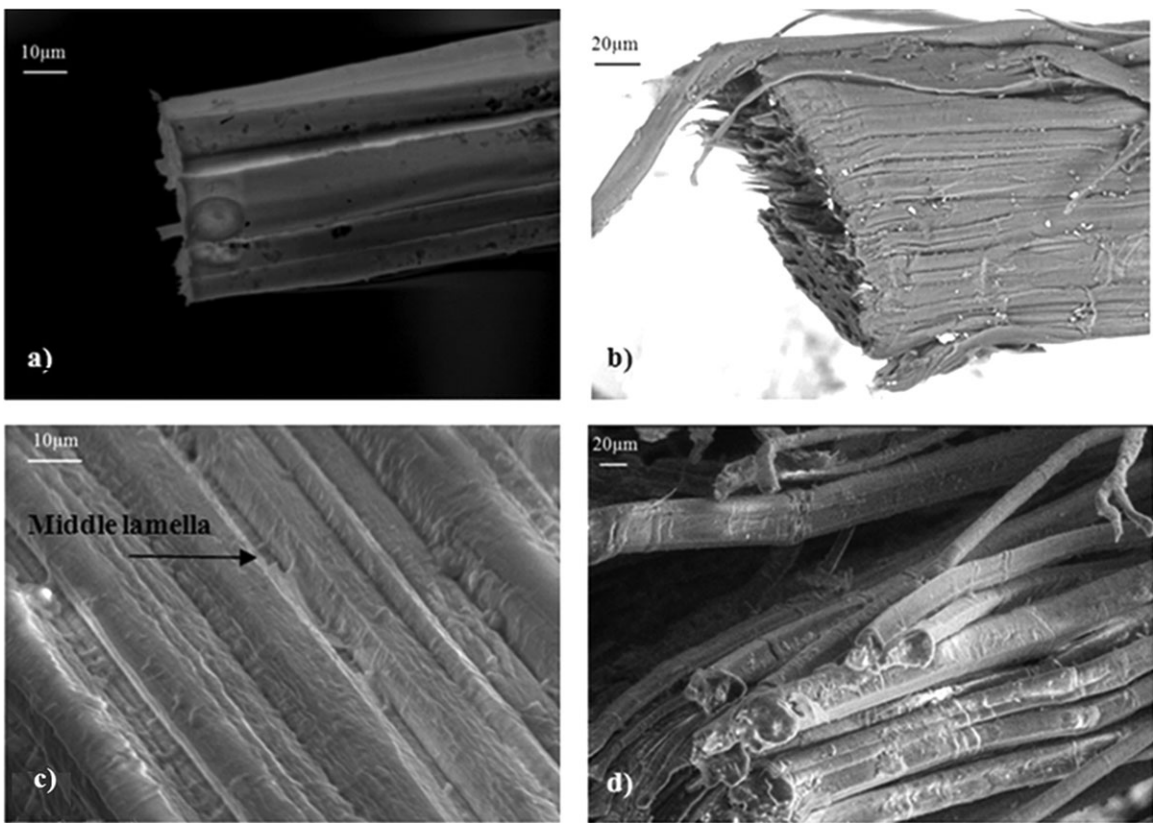


**Figure 7.** SEM pictures of (a) jute, (b) sisal, (c) flax, and (d) hemp bundles.

Table V. Densities of the Four Studied Fibers Determined through Pycnometry

| Fiber | Density (kg/m$^3$) |
|---|---|
| Sisal | 1058.2 ± 80.8 |
| Jute | 1201.8 ± 55.4 |
| Hemp | 1402.9 ± 84.8 |
| Flax | 1358.9 ± 20.6 |

This hypothesis will be checked later with the analysis of aging test performed on such fibers (see section "Experimental results in immersion").

**SEM Analysis.** SEM observations of the longitudinal surface of the four kinds of fibers were realized. Pictures of jute, sisal, flax, and hemp fibers are presented in different scales on Figure 7(a–d), respectively. They show the complex structure of natural fibers. It consists of several elementary fibers linked together by the middle lamella composed by pectin that give strength to the bundle. In this area, moisture sorption is enhanced. In Figure 7(c), the hydrophilic lamella is pointed by the arrow.

**Pycnometry.** Results deduced from pycnometry tests are presented in Table V. The densities obtained for dried sisal, jute, flax, and hemp at room temperature were 1058.2 (±80.8), 1201.8 (±55.4), 1402.9 (±84.8), and 1358.9 (±20.6) kg/m$^3$, respectively. The density is in the same order for all fibers. These values are consistent to other natural fibers like palm (1030 kg/m$^3$) and coconut (1150 kg/m3) and same fibers investigated by others authors.[4,23] All vegetal fibers present densities much lower than glass fibers (2500 kg/m$^3$). As a consequence, they have interesting specific mechanical properties to compete with glass fibers as presented in Table I.

The densities deduced from pycnometry analysis are necessary to calculate the water concentration in fibers from the time-dependent mass uptake collected during aging tests (see section "Experimental results in immersion").

**Kinetic's Diffusion Model**

Classical diffusion models used to predict diffusion phenomenon inside polymers (Fick's law, dual-stage Fick's law, and Langmuir model) have been used for interpreting our experimental results.

**Fick's Law.** The traditional Fickian diffusion model[47] used to predict transport phenomena in numerous environments is the most common model used for predicting the diffusion of moisture in polymeric resins. Besides, the model is consistent with the so-called free volume theory.[48]

For the purpose of modeling, fibers have been assumed to be assimilated as a full homogenous cylinder the radius $r$ of which is very small compared to its length. In the case when a long circular cylinder is considered, in which diffusion is radial (one-dimensional case), the moisture concentration $C$ is then a function of radius $r$ and time $t$, only. The corresponding diffusion equation writes as follows:[49]

$$\frac{\partial C}{\partial t} = D\left(\frac{1}{r}\frac{\partial C}{\partial r} + \frac{\partial^2 C}{\partial r^2}\right) \tag{3}$$

where $D$ is the diffusion coefficient.

Indeed, the integration of the analytical solution of eq. (3), over the cylinder of radius $r = a$ yields the following expression for the moisture uptake:

$$\frac{M_t}{M_\infty} = 1 - \sum_{n=1}^{\infty} \frac{4}{a^2\alpha_n^2}\exp(-D\alpha_n^2 t) \tag{4}$$

where $\alpha_n$ are the roots of the first species of Bessel's function at order 0, $M_t$ is the moisture content at time $t$, and $M_\infty$ is the moisture content at infinite time.

By minimizing the agreement between the experimental results and the moisture uptake predicted owing to eq. (4), we determined both the Fickian diffusion coefficients and the saturation mass uptake ($M_\infty$) for each investigated fiber.

**Dual-Stage Fick's Law.** The dual-stage moisture transport model has also been successfully used for predicting and interpreting aging test, as shown, for instance, in Ref. 20. In the case of an anomalous moisture uptake, Loh et al. developed a dual-stage uptake model consisting of two Fickian diffusion kinetics occurring in parallel. Both the Fickian diffusion models use eq. (5) with separate diffusion coefficient ($D_1$ and $D_2$) and saturation levels ($M_{\infty 1}$ and $M_{\infty 2}$), respectively. The sum of each saturation level gives the total moisture absorption capacity of the specimen in the steady state of the diffusion process [eq. (6)].

$$\begin{aligned} M_t = {} & M_{\infty 1}\left(1 - \sum_{n=1}^{\infty}\frac{4}{a^2\alpha_n^2}\exp(-D_1\alpha_n^2 t)\right) \\ & + M_{\infty 2}\left(1 - \sum_{n=1}^{\infty}\frac{4}{a^2\alpha_n^2}\exp(-D_2\alpha_n^2 t)\right) \end{aligned} \tag{5}$$

$$M_{\infty 1} + M_{\infty 2} = M_\infty \tag{6}$$

**Langmuir Law or Two-Phase Model of Carter and Kibler.** This model was developed 35 years ago by Carter and Kibler.[50] It is based on the Langmuir theory of adsorption on surface. In this model, the moisture absorption can be explained quantitatively by assuming that absorbed moisture consists of both mobile and bound phases. Molecules of the mobile phase diffuse with a concentration and stress independent diffusion coefficient $D_\gamma$, and are absorbed (become bound) with a probability per unit time $\gamma$ at certain sites (e.g., voids within the polymer, hydrogen bonding, and heterogeneous morphology). Molecules are emitted from the bound phase, thereby becoming mobile, with a probability per unit time $\beta$.

For the one-dimensional case, in a homogeneous cylinder of diameter $r$, the molecular number densities at time $t$ satisfy the following coupled set of equations:

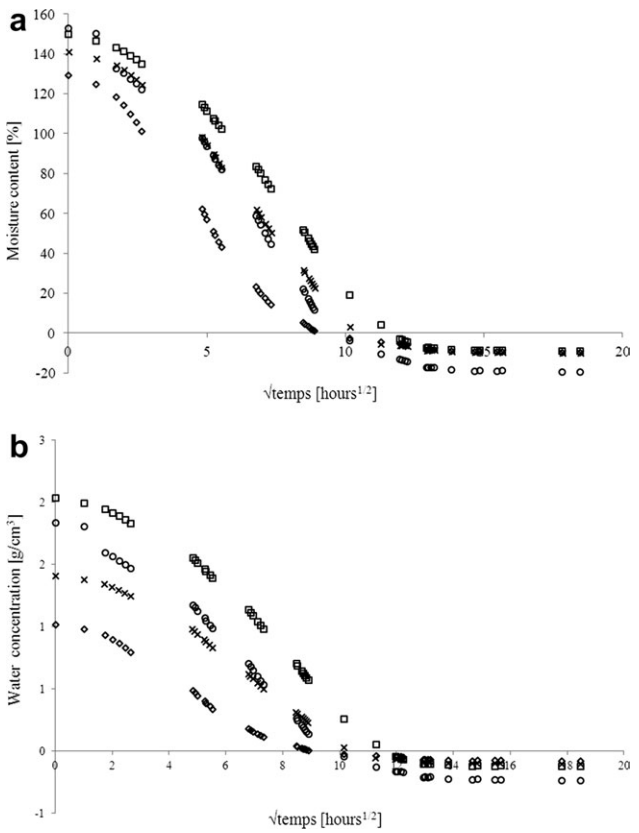


**Figure 8.** Desorption curves of natural fibers (×flax, □ hemp, ◇sisal, ○jute) (a) water content, (b) water concentration.

$$\begin{cases} \dfrac{\partial n}{\partial t} = D\left(\dfrac{\partial^2 n}{\partial r^2} + \dfrac{1}{r}\dfrac{\partial n}{\partial r}\right) + \dfrac{\partial N}{\partial t} & (7) \\ \dfrac{\partial N}{\partial t} = \gamma n - \beta N & (8) \end{cases}$$

$$\gamma n\infty = \beta N\infty \quad (9)$$

where $n$ is the number of mobile molecules per unit volume and $N$ is the number of bound molecules per unit volume.

Theses coupled equations are numerically solved by finite difference. We tested different value of the three parameters $D\gamma$, $n$, and $\beta$. The triplet that minimizes the square differences between experimental and theoretical results constitutes the best parameters.

**Experimental Results in Immersion.** The desorption kinetics (after immersion) of the four fibers are represented on Figure 8. In Figure 8, the mass at $t = 0$ corresponds to the relative mass gain reaches after 11 days of immersion ($M_s$). $M_s$ is calculated with eq. (2) (see section "specimen aging"), using $M_0$ as the initial mass before immersion. Then, the relative mass loss against root square time is plotted. Results obtained for the moisture content are displayed on Figure 8(a) whereas water concentration is depicted on Figure 8(b). Water concentration is deduced from moisture content and the densities measured by pycnometry (see section "Pycnometry").

After immersion, the relative mass gain reaches 130% for sisal, 149% for hemp, 141% for flax, and 153% for jute in 11 days.

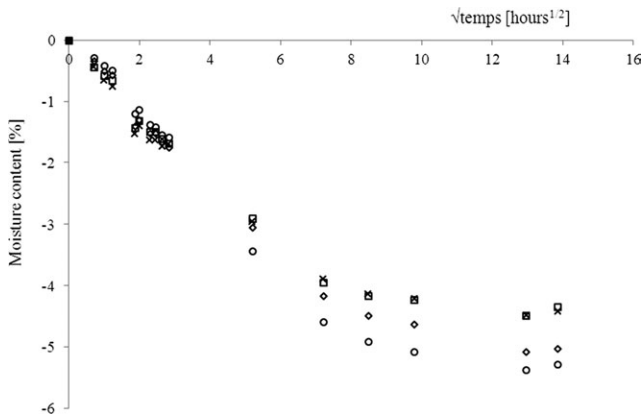


**Figure 9.** Determination of initiale water in fibers (×flax, □ hemp, ◇sisal, ○jute).

This value could be compared to the works of Bessadok et al.[12] The authors found a mass gain of 140% for Alfa fibers in immersion. All fibers have a similar diffusive behavior. Indeed, characterization achieved previously on the four fibers did show strong similarities of their chemical footprint (IR spectroscopy) as well as their microstructure (SEM). X-ray analysis performed has shown differences in the crystallinity indices because of difference in cellulose content. In the aging tests performed here, the correlation between crystallinity and water uptake in cellulosic materials supposed by Nakamura et al.[46] is not clear. In bundles of fibers, which contain pore and voids the free water could penetrate inside and could be trapped. Moreover, water diffusion is privileged in the middle lamella. This could explain the similarity of the equilibrium water content for the four fibers despite some different crystallinity index

The curves displayed in Figure 8 have a sigmoid shape that can be the result of a delay time in the establishment of water concentration equilibrium at the fiber surface. After total drying of the sample, the initial weight is not reached [Figure 8(a)]. There is a relative mass loss of about 10% compared to the initial weight for flax, hemp, and sisal. Such mass loss could be attributed to the existence of water content in fibers at the initial stage, corresponding to the ambient relative humidity. Drying

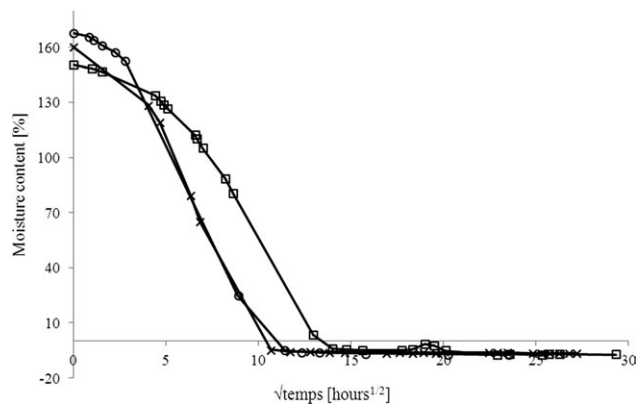


**Figure 10.** Cycling results for hemp jute fiber bundles (□1st cycle, × 2nd cycle, ○3rd cycle).

**Table VI.** Diffusion Parameters Determined According to Each Model

| Model | Parameter | Hemp | Jute | Flax | Sisal |
|---|---|---|---|---|---|
| Fick | $D$ ($mm^2/s$) | $4.00\ 10^{-6}$ | $1.12\ 10^{-6}$ | $1.19\ 10^{-6}$ | $2.14\ 10^{-6}$ |
| Dual stage fick | $D_1$ ($mm^2/s$) | $5.29\ 10^{-6}$ | $2.33\ 10^{-6}$ | $2.11\ 10^{-6}$ | $4.00\ 10^{-6}$ |
| | $D_2$ ($mm^2/s$) | $5.80\ 10^{-7}$ | $2.30\ 10^{-7}$ | $2.11\ 10^{-7}$ | $4.38\ 10^{7}$ |
| Langmuir | $D\gamma$ ($mm^2/s$) | $5.6\ 10^{-6}$ | $5.9\ 10^{-6}$ | $6.8\ 10^{-6}$ | $9.1\ 10^{-6}$ |
| | $\beta$ ($s^{-1}$) | $4.25\ 10^{-6}$ | $4.95\ 10^{-6}$ | $5.75\ 10^{-6}$ | $8.25\ 10^{-6}$ |
| | $M_\infty$ (%) | 63 | 67.8 | 62.5 | 60.6 |

of other fiber samples in desiccators at room temperature (Figure 9) shows a relative mass loss of about 6%. This initial water is underlined on the FTIR spectra (see section "FTIR spectroscopy"). With jute, the dried fiber mass (after total desorption) is 20% lower than the initial weight. In this case, to rule out the hypothesis of damages in jute fiber, three cycles of absorption/desorption were realized. Jute fiber kinetics for the three cycles are presented on the Figure 10, only in desorption. Curves do not present any damage. After drying, they always recover the same weight. However, the saturation mass is not exactly the same for all cycles. This could be explained by the man made drying after sample was thrown of water: that stage of the characterization process is actually rather difficult to reproduce in practice.

The three models described before have been used to fit the experimental results. The best adjustment has been achieved by using a classical least-squares method that minimizes the sum of squared residuals, resulting in the difference between experimental results and the fitted value provided by the model. Parameters obtained by identification for each model and each fiber are listed in Table VI. The predictive curves are presented in Figure 11, where the full line stands for the Fickian model, whereas the dashed line corresponds to Langmuir-type model (predictive curves for dual-stage Fickian model are not presented here because the shape was found very close to Fickian results). To achieve the numerical simulations according to the predictive models, we have made some changes in the graphical representation of the results. First, initial mass $M_0$ has been taken as the saturated fiber mass and, second, desorption curves have been commuted in absorption kinetics assuming the hypothesis that absorption and desorption behavior in such fibers is similar. The corresponding representation of the experimental results is depicted in the Figure 11 through the diamonds curves.

The results show that the classical Fickian diffusion model with a single, constant, diffusion coefficient fails to properly

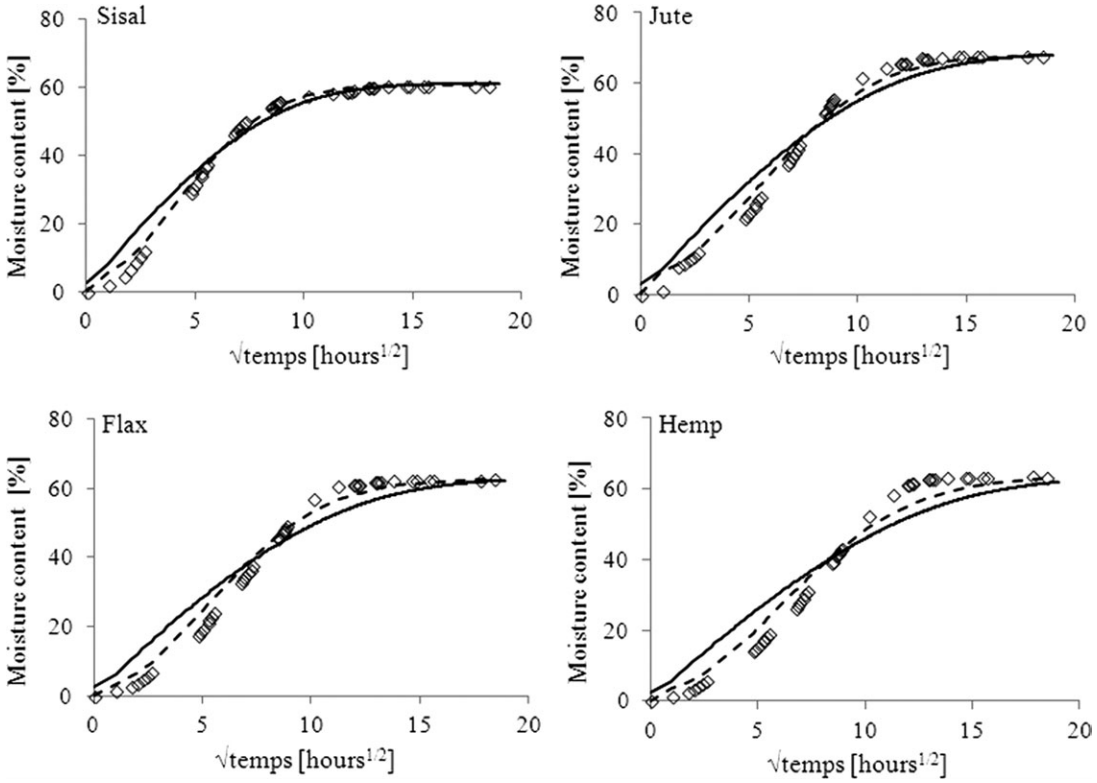


**Figure 11.** Results for diffusion in immersion (◇ experimental results, --- Langmuir's model, — Fick's model).

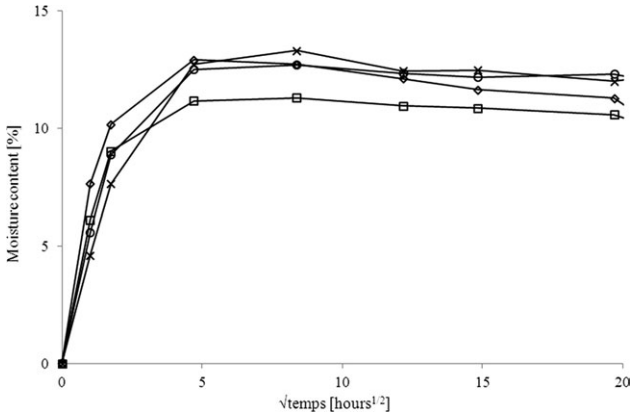


**Figure 12.** Absorption kinetics of natural fibers in hygrothermal conditions: RH = 80%, $T = 23°C$ (×flax, □ hemp, ◇sisal, ○jute).

reproduce the experimental uptake curves in all cases. On the opposite, the model originally developed by Carter and Kibler describes very well the kinetics of water uptake in these natural fibers in condition of immersion. Similar diffusion coefficients $D\gamma$ were found for the four fibers. In the immersion condition, there are no data available in literature to be compared with our results. Diffusion coefficient for sisal is almost two times higher than the others. This could be linked to the much important amorphous part inside sisal that makes easier the diffusion. The $\beta$ coefficient that is the probability of a bound water molecule to become mobile is also higher for sisal. Saturation moisture contents are comparable, in light of the weak reproducibility of the measurement. The two phases of water considered in the model could be linked to Hatakeyama's works[51] dealing with the different kind of water interacting with cellulosic materials. These different kinds of water could be separated in two categories. First, the free water (bulk water and capillarity water) that could constitute the mobile phase in the Carter and Kibler model and the bound water (nonfreezing and freezing bound water), which could be the bonded phase in the diffusion model. By performing cooling of hydrated cellulose in differential scanning calorimetry, they could find the amount of bound and free water inside samples. Thereby, the technique developed in Hatakeyama's works could be an experimental solution to validate our model.

**Experimental Results in Relative Humidity (RH = 80%).** Absorption kinetics for fibers aged in an environmental chamber with a relative humidity of 80% are presented in Figure 12. The curves are typical of a Fickian diffusion. The corresponding diffusion parameters have been calculated by using eq. (4). They are presented in Table VII. In previously published works, Mannan et al.[13] found a diffusion coefficient of 3.38 $10^{-7}$ $mm^2 \cdot s^{-1}$ for jute fibers in condition of 51% relative humidity. As for immersion conditions, all the fibers have similar diffusion parameters.

**Table VII.** Fickian Parameters for Fibres Aged in Hygro-Thermal Conditions RH = 80%, $T = 23°C$

| | Hemp | Jute | Flax | Sisal |
|---|---|---|---|---|
| $M_\infty$ (%) | 10.5 | 12.3 | 12.0 | 11.2 |
| $D$ ($mm^2/s$) | $2.27\ 10^{-4}$ | $4.02\ 10^{-4}$ | $2.00\ 10^{-4}$ | $1.17\ 10^{-4}$ |

## CONCLUSION

First, a characterization of four natural fibers has been achieved by using different technical analysis. The characterization enabled us to identify the composition of fibers, estimate the crystallinity degree, and observe the complex structure of fibers. Despite their different origins, the four fibers have a similar structure. Then, they have a similar diffusive behavior.

By performing aging test, we have also shown that natural fibers exposed to moisture in immersion or vapor humidity conditions do not exhibit the same diffusive behavior. Langmuir theory actually describes very well diffusion inside fibers immersed in liquid water whereas the same fibers follow a Fickian diffusion in the case when they are exposed to vapor during relative humidity aging. The mass gain in immersion is widely more important than in an environment at 80% relative humidity. This gap can be explained by the specimen's geometry. Free volume in such fibers is important and liquid water could be trapped inside pores. In vapor conditions, it is possible that some water molecules remain in a gaseous state within the void parts of the samples. Because gaseous water could be released easily, the mass gain is less important. In both cases, there is no damage according to the absorption and desorption cycles.

In the case of immersion, the observed curvature of the time dependent weight-gain could be attributed to effects induced by mechanical states on the diffusion of moisture. Upcoming investigations will be focused on the use of more advanced multiphysics theoretical approaches dedicated to the modeling of the moisture uptake occurring while the heterogeneous, local swelling experienced by the polymer is accounted for. Such a model, recently published in the literature by Sar et al.,[52] should provide a more realistic framework for interpreting the aging tests achieved on natural fibers, in particular in the cases when immersion conditions are considered.

## ACKNOWLEDGMENTS

The authors would like to acknowledge Dr. Annick Perronnet for her help during SEM sessions.

## REFERENCES

1. Summerscales, J.; Dissanayake, N.; Hall, W.; Virk, A. S. *Composite Part A.* **2010**, *41*, 1329.
2. Wambua, P.; Ivens, J.; Verpoest, I. *Compos. Sci. Technol.* **2003**, *63*, 1259.
3. Suddell, B. C.; Evans, W. J. In Biopolymers & Their Bio-Composites; Mohanty, A. K.; Misra, M.; Drzal, L. T., Eds.; CRC Press: Boca Raton, FL, **2005**, p. 231.
4. Bledzki, A. K.; Gassan, J. *Prog. Polym. Sci.* **1999**, *24*, 221.
5. Stamboulis, A.; Baillie, C. A.; Peijs, T. *Composites Part A.* **2001**, *32*, 1105.

6. Lee, J. M.; Pawlak, J. J.; Heitmann, J. A. *Mater. Charact.* **2010**, *61*, 507.
7. Rangaraj, S. V.; Smith, L. *J. Thermoplast. Compos. Mater.* **2000**, *13*, 140.
8. Costa, F. H. H. M.; D'Almeida, J. R. M. *Polym-Plast. Technol.* **1999**, *38*, 1081.
9. Mishra, S.; Naik, J.; Patil Y. *Compos. Sci. Technol.* **2000**, *60*, 1729.
10. Hill, C. A. S.; Abdul Khalil, H. P. S.; Hale, M. D. *Ind. Crop. Prod.* **1998**, *8*, 53.
11. Alix, S.; Lebrun, L.; Morvan, C.; Marais, S. *Compos. Sci. Technol.* **2011**, *71*, 893.
12. Bessadok, A.; Marais, S.; Gouanvé, F.; Colasse, L.; Zimmerlin, I.; Roudesli, S.; Metayer, M. *Compos. Sci. Technol.* **2007**, *67*, 685.
13. Mannan, Kh. M.; Talukder M. A. I. *Polymer* **1997**, *38*, 2493.
14. Gouanve, F.; Marais, S.; Bessadok, A.; Langevin, D.; Metayer M. *Eur. Polym. J.* **2007**, *43*, 586.
15. Jedidi, J.; Jacquemin, F.; Vautrin, A. *Compos. A* **2006**, *37*, 636.
16. Autran, M.; Pauliard, R.; Gautier, L.; Mortaigne, B.; Mazeas, F.; Davies P. *J. Appl. Polym. Sci.* **2002**, *84*, 2185.
17. Zhou, J.; Lucas J. P. *Polymer* **1999**, *40*, 5505.
18. Roy, S.; Xu, W. X.; Park S. J.; Liechti K. M. *J. Appl. Mech.* **2000**, *67*, 391.
19. Popineau, S.; Rondeau-Mouro, C.; Sulpice-Gaillet, C.; Shanahan M. E. R. *Polymer* **2006**, *46*, 10733.
20. Loh, W. K.; Crocombe, A. D.; Abdel Wahab, M. M.; Ashcroft I. A. *Int. J. Adhes. Adhes.* **2005**, *25*, 1.
21. Kohler, R.; Dück, R.; Ausperger, B.; Alex R. *Compos. Interfaces* **2003**, *10*, 255.
22. Jacquemin, F.; Fréour, S.; Guillén R. *Compos. Sci.Technol.* **2006**, *66*, 397.
23. Satyanarayana, K. G.; Wipych, F. In Engineering biopolymers: Homopolymers, Blends and Composites. Fakirov, S., Bhattacharyya, D., Eds.; Hanser Publishers: Munich, **2007**, p.3.
24. Oksman, K.; Skrifvars, M.; Selin, J. F. *Compos. Sci. Technol.* **2003**, *63*, 1317.
25. Gorshkova, T.; Gurjanov, O.; Mikshina, P.; Ibragimova, N.; Mokshina, N.; Salnikov, V.; Ageeva, M. V.; Amenitskii, S. I.; Chernova, T. E.; Chemikosova, S. B., *Russ. J. Plant Phys.* **2010**, *57*, 328.
26. Hearle, J. W. S. *J. Appl. Polym. Sci.* **1963**, *7*, 1207.
27. Morvan, C.; Andème-Onzighi, C.; Girault, R.; Himmelsbach, D. S.; Driouich, A.; Akin, D. E. *Plant Physiol. Biochem.* **2003**, *41*, 935.
28. Baley, C. *Compos. A* **2002**, *33*, 939.
29. Siroky, J.; Blackburn, R. S.; Bechtold, T.; Taylor, J.; White, P. *Cellulose* **2010**, *17*, 103.
30. O'Connor, R. T.; DuPré, E. F.; Mitcham D. *Text Res. J.* **1958**, *28*, 382.
31. Nelson, M. L.; O'Connor, R. T. *J. Appl. Polym. Sci.* **1964b**, *8*, 1325.
32. Segal, L.; Creely, J. J.; Martin, A. E.; Conrad, C. M. *Text. Res. J.* **1959**, *29*, 786.
33. Thygesen, A.; Oddershede, J.; Lilholt, H.; Thomsen, A. B.; Stahl K. *Cellulose* **2005**, *12*, 563.
34. Pratten, N. A. *J. Mater. Sci.* **1981**, *16*, 1737.
35. Liang, C. Y.; Marchessault, R. H. *J. Polym. Sci.* **1959**, *39*, 269.
36. Marchessault, R. H. *Pure Appl. Chem.* **1962**, *5*, 107.
37. Nelsson, M. L.; O'Connor, R. T. *J.Appl. Polym. Sci.* **1964**, *8*, 1311.
38. Kondo, T. *Cellulose* **1997**, *4*, 281.
39. De Rosa, I. M.; Kenny, J. M.; Puglia, D.; Santulli, C.; Sarasini, F. *Compos. Sci. Technol.* **2010**, *70*, 116.
40. Olson, A. M.; Salmen, L. *Carbohydr. Res.* **2004**, *339*, 813.
41. Davies, G. C.; Bruce, D. M. *Text. Res. J.* **1998**, *60*, 623.
42. Cousins, W. J. *Wood Sci. Technol.* **1978**, *12*, 1319.
43. Sarko, A.; Muggli, R. *Macromolecules* **1974**, *7*, 486.
44. Park, S.; Baker, J. O.; Himmel, M. E.; Parilla, P. A.; Johnson, D. K. *Biotechnol Biofuels*, **2010**, *3*, 10.
45. Le Duigou, A. Contribution à l'étude des biocomposites. Ph.D. Thesis, Université de Bretagne Sud, **2010**.
46. Nakamura, K.; Hatakeyama, T.; Hatakeyama, H. *Text. Res. J.* **1981**, *51*, 607.
47. Fick A. Ueber Diffusion. *Annal. Phys.* **1855**, *170*, 59.
48. Eyring, H. Viscosity. *J. Chem. Phys.* **1936**, *4*, 283.
49. Crank, J. The Mathematics of Diffusion. Clarendon Press: Oxford, **1975**.
50. Carter, H.; Kibler, K. *J. Compos. Mater.* **1978**, *12*, 118.
51. Hatakeyama, H.; Hatakeyama, T. *Thermochim. Acta.* **1998**, *308*, 3.
52. Sar, B. E.; Fréour, S.; Davies, P.; Jacquemin, F. *Eur. J. Mech.* **2012**, *36*, 38.